Cell Reports

Report

Alternative Translation Initiation Generates a Functionally Distinct Isoform of the Stress-Activated Protein Kinase MK2

Graphical Abstract

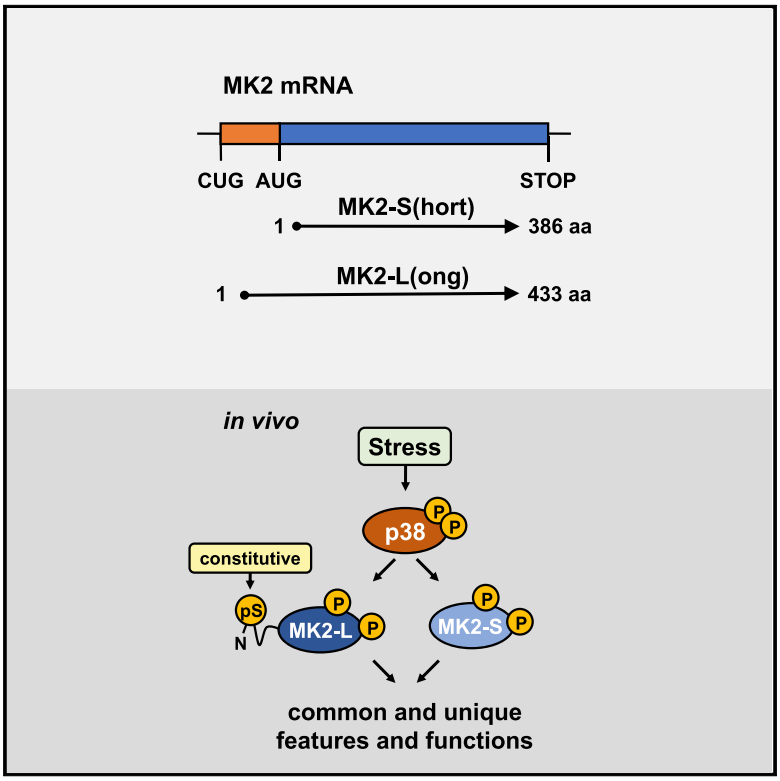

Highlights

- The MK2 mRNA contains an in-frame upstream CUG translation initiation site
- An N-terminal extended isoform of the protein kinase MK2 is consequently translated
- This isoform has unique and shared properties compared to the canonical isoform
- The extended N terminus of long MK2 is phosphorylated at a defined serine residue

Authors

Philipp Trulley, Goda Snieckute, Dorte Bekker-Jensen, ..., Simon Bekker-Jensen, Matthias Gaestel, Christopher Tiedje

Correspondence

sbj@sund.ku.dk (S.B.-J.), gaestel.matthias@mh-hannover.de (M.G.), tiedje@sund.ku.dk (C.T.)

In Brief

In the present study, Trulley et al. identify a N-terminal extended long isoform of the stress-activated protein kinase MK2 that constitutively arises from alternative translation initiation within the known MK2 mRNA. The long isoform has unique and shared molecular properties, compared to the canonical short isoform.

Trulley et al., 2019, Cell Reports *27*, 2859–2870
June 4, 2019
https://doi.org/10.1016/j.celrep.2019.05.024

CellPress

Cell Reports
Report

Alternative Translation Initiation Generates a Functionally Distinct Isoform of the Stress-Activated Protein Kinase MK2

Philipp Trulley,[1,7] Goda Snieckute,[2,7] Dorte Bekker-Jensen,[3] Manoj B. Menon,[1,6] Robert Freund,[1] Alexey Kotlyarov,[1] Jesper V. Olsen,[3] Manuel D. Diaz-Muñoz,[4,5] Martin Turner,[5] Simon Bekker-Jensen,[2,*] Matthias Gaestel,[1,*] and Christopher Tiedje[1,2,8,*]

[1]Institute of Cell Biochemistry, Hannover Medical School (MHH), Carl-Neuberg-Str. 1, 30625 Hannover, Germany
[2]Center for Healthy Aging, Department of Cellular and Molecular Medicine, University of Copenhagen, Blegdamsvej 3B, 2200 Copenhagen N, Denmark
[3]Mass Spectrometry for Quantitative Proteomics, Proteomics Program, The Novo Nordisk Foundation Center for Protein Research, Faculty of Health and Medical Sciences, University of Copenhagen, Blegdamsvej 3B, 2200 Copenhagen N, Denmark
[4]Centre de Physiopathologie Toulouse-Purpan, INSERM UMR1043/CNRS U5282, Toulouse 31300, France
[5]Lymphocyte Signalling and Development, The Babraham Institute, CB22 3AT Cambridge, UK
[6]Present address: Kusuma School of Biological Sciences, Indian Institute of Technology, Hauz Khas, New Delhi, India
[7]These authors contributed equally
[8]Lead Contact
*Correspondence: sbj@sund.ku.dk (S.B.-J.), gaestel.matthias@mh-hannover.de (M.G.), tiedje@sund.ku.dk (C.T.)
https://doi.org/10.1016/j.celrep.2019.05.024

SUMMARY

Alternative translation is an important mechanism of post-transcriptional gene regulation leading to the expression of different protein isoforms originating from the same mRNA. Here, we describe an abundant long isoform of the stress/p38^{MAPK}-activated protein kinase MK2. This isoform is constitutively translated from an alternative CUG translation initiation start site located in the 5′ UTR of its mRNA. The RNA helicase eIF4A1 is needed to ensure translation of the long and the known short isoforms of MK2, of which the molecular properties were determined. Only the short isoform phosphorylated Hsp27 *in vivo*, supported migration and stress-induced immediate early gene (IEG) expression. Interaction profiling revealed short-isoform-specific binding partners that were associated with migration. In contrast, the long isoform contains at least one additional phosphorylatable serine in its unique N terminus. In sum, our data reveal a longer isoform of MK2 with distinct physiological properties.

INTRODUCTION

Post-transcriptional gene regulation (PTGR) constitutes an important toolbox used to shape gene expression upon intra- and extracellular cues. PTGR impacts on mRNA processing, localization, export, stability, and translation. Canonical translation of mRNA starts on AUG translation initiation sites (TISs) that are recognized by ribosomes through scanning of the 5′ UTR leader sequence and is dependent on the cap structure. The entire translation initiation mechanism is tightly regulated (Sonenberg and Hinnebusch, 2009) and can be influenced by sequences in the 5′ UTR-bearing internal ribosomal entry sites (IRESs), secondary structures, or upstream open reading frames (uORFs) or by "leaky scanning" of sequences preceding the initiator AUG (Kozak sequence), leading to the usage of alternative start codons that result in alternative protein isoform translation (Barbosa et al., 2013; Fritsch et al., 2012; Hinnebusch et al., 2016). The mechanisms by which ribosomes select non-AUG codons for translation initiation might rely on auxiliary initiation factors and RNA helicases such as eIF4A1, eIF2A, or Ddx3 (Guenther et al., 2018; Modelska et al., 2015; Sendoel et al., 2017; Starck et al., 2012; Wolfe et al., 2014). Translation events starting at these non-AUG start codons have led to the determination of alternative translation initiation sites (aTISs) (Wan and Qian, 2014; Wegrzyn et al., 2008). Taken together, these features of translation explain, in part, how proteome diversity in cells can be generated from a limited number of transcripts.

Protein kinases and associated signal transduction pathways play an important role in regulating transcriptional and post-transcriptional events. A well-characterized pathway is the p38^{MAPK}-MK2-signaling module. The p38^{MAPK}-activated protein kinase MK2 (or MAPKAPK2) phosphorylates substrates such as the RNA-binding protein and PTGR master regulator tristetraprolin (TTP) and the transcription factor serum response factor (SRF) (Menon and Gaestel, 2018). Numerous reports characterize the diverse functions of MK2 in inflammation and stress signaling (Gaestel, 2013), also suggesting its role as a checkpoint kinase in cancer (Reinhardt et al., 2011). Powerful tools for these studies are the MK2 knockout (MK2 KO) (Kotlyarov et al., 1999) and the MK2/3 double knockout (MK2/3 DKO) (Ronkina et al., 2007) mouse models. Among them, the DKO model seems superior over the single KO, as it eliminates compensatory effects of the MK2-related kinase MK3 on MK2 functions (Ronkina et al.,

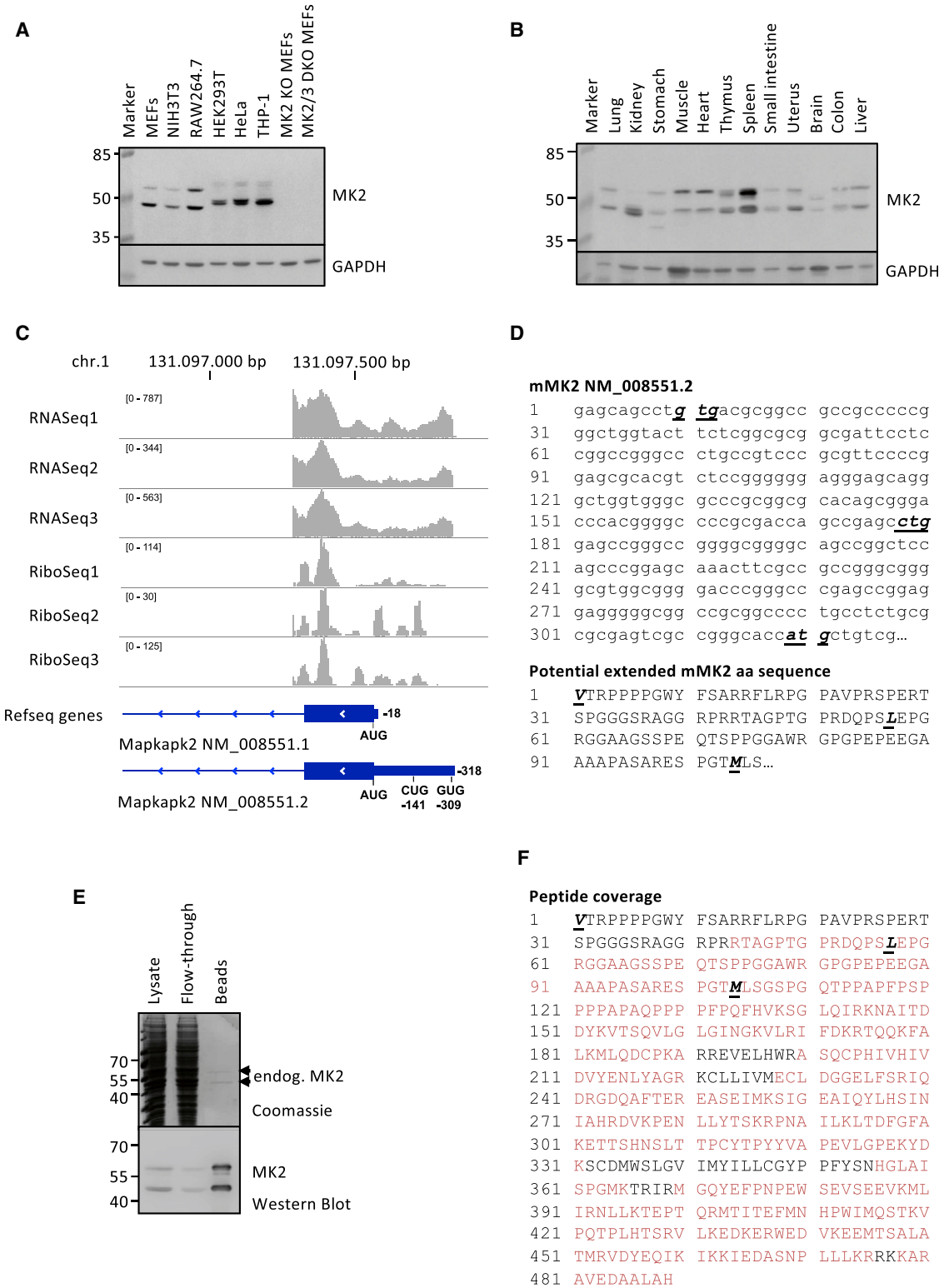

Figure 1. Translation of MK2 from an Alternative Start Codon in Its 5′ UTR

(A) Expression profiling of MK2 in different murine and human cell lines by western blot.

(B) Expression profiling of MK2 in mouse organs by western blot.

(legend continued on next page)

2007). MK2 deletion phenotypes range from defects in immediate early gene responses over impaired cytokine production and regulation of apoptosis and/or necroptosis to non-coding RNA regulation and defects in migration. They could be linked to specific substrates of MK2, such as TTP (Tiedje et al., 2016) and SRF (Ronkina et al., 2011), as well as RIPK1 (Dondelinger et al., 2017; Jaco et al., 2017; Menon et al., 2017), RBM7 (Blasius et al., 2014; Tiedje et al., 2015), and Hsp25/27 (Hoffman et al., 2017).

Western blot detection of endogenous MK2 often gave two bands where only the lower band represented the apparent molecular mass of the protein kinase (Cano et al., 1996; Stokoe et al., 1992). Interestingly, ectopically expressed MK2 does not display the second, slower migrating band. To date, no information about the nature of this MK2 isoform expression is available. We now show that the long MK2 isoform constitutively arises from alternative translation of an in-frame upstream CUG alternative translation initiation site in the highly conserved GC-rich 5′ UTR and characterize the properties of this isoform.

RESULTS

Translation of MK2 from an Alternative Start Codon in the 5′ UTR of Its mRNA

MK2 is ubiquitously expressed (Gaestel, 2013), and when analyzing its expression in different cell lines or in mouse tissues by western blotting, a multiple band pattern is detected (Figures 1A, 1B, and S1). Of note, the ratio of expression of these bands varies between tissues and cell lines. In murine cells and tissues, two predominant bands can be detected in western blot analysis by using an anti-MK2 antibody directed toward the C terminus of human MK2 (Figures 1A and 1B). The low-molecular-weight band corresponds to the hitherto known open reading frame (ORF) of the gene, whereas the origin and function of the slower migrating band are obscure, and only one transcript existed in the NCBI database (NCBI: NM_008551.2). Importantly, both bands were found to be absent in cells from MK2 KO (described in Kotlyarov et al., 1999) and MK2/3 DKO mice (described in Ronkina et al., 2007) (Figures 1A and S1A). In human cell lines, two dominating bands of around 55 kDa, together with two less intense bands at around 65 kDa, were detected (Figures 1A, S1C, and S1D). Two similar human MK2 transcripts (GenBank: NM_004759.4 and NM_032960.3) can be found in the database and arise from alternative splicing. Short hairpin RNA (shRNA)-mediated knockdown of human MK2 in HT29 cells removed all of these bands, confirming that they were derived from the same gene (Figure S1D). For the murine MK2-related protein kinase MK3, only one specific protein product is detected that is absent in MK2/3 DKO cells (Figures S1A and S1B). From these data, we concluded that the different MK2 protein bands could be assigned to distinct protein isoforms that may originate from different post-translational modifications of MK2, alternative splicing, or alternative translation events.

To test the hypothesis of the existence of alternative translation products, we exploited existing RNA-sequencing (RNA-seq) and ribosome-footprinting (RiboSeq) data from different cell lines. Initially, data from murine bone-marrow-derived macrophages (BMDMs) (Tiedje et al., 2016) were reanalyzed and revealed the existence of an MK2 transcript with an extended 5′ UTR that also contained several ribosome footprints (RFPs) within this region (Figure 1C). This supported the idea of the existence of alternative translation events in the 5′ UTR of mouse MK2. In fact, an MK2 transcript that corresponded to the transcript length we detected by RNA-seq was recently deposited at NCBI (NCBI: NM_008551.2) and replaced the previously annotated transcript having only a very short, 18-nt 5′ UTR (NCBI: NM_008551.1; Figure 1C). The analysis of this transcript showed a potential in-frame extension of the hitherto known MK2 ORF in the upstream direction (Figure 1D). Within this extension, we found two putative alternative translation initiation sites at positions −141 and −309, coding for leucine (CUG) and valine (GUG), respectively. The CUG and GUG are surrounded by the alternative Kozak sequences GCCGAGC*CUG*GAG and GCAGCCT*GUG*ACG (Wegrzyn et al., 2008). Consistent with the western blot results, RFPs and sequence analyses revealed an in-frame extension in the 5′ UTR of the human MK2 transcript bearing the two alternative start codons CUG and GUG (Figures S2A and S2B). Interestingly, in the human transcript, the CUG is almost the same distance from the AUG (−144 bp, −48 aa) as in the mouse transcript. Overall, more than 80% sequence identity within the first 200 bp upstream of the start AUG codon exists between the murine and human 5′ UTRs (Figure S2C). Further sequence analyses showed that the 5′ UTR extension is evolutionary conserved among species, indicating a distant origin for alternative translation of MK2 isoforms (Data S1). This observation was supported by analyzing published RiboSeq datasets of murine and human cells that were treated with cycloheximide, harringtonine, or lactimidomycin before sequencing of ribosome-protected mRNA fragments (Fields et al., 2015; Fijalkowska et al., 2017; Gawron et al., 2016; Ingolia et al., 2012; Oh et al., 2016; Sendoel et al., 2017; Valentin-Vega et al., 2016). Since mRNA-bound ribosomes are frozen at translation initiation start sites by these treatments, as previously exemplified in pioneering RiboSeq studies (Ingolia et al., 2011; Lee et al., 2012), the existence of footprints in the 5′ UTR of MK2 strongly argues for alternative translation events. Indeed, we could

(C) Genomic tracks of RNASeq and RiboSeq datasets (GEO: GSE81250) for the old MK2 transcript NM_008551.1 and its most recent annotated transcript version, NM_008551.2. The positions of potential alternative translation initiation sites (aTISs) within the 5′ UTR and the AUG initiation sites are marked.

(D) The murine MK2 5′ UTR nucleotide sequence and its putative extended in-frame N-terminal amino-acid sequence. The alternative translation initiation sites are marked in bold and italics within both sequences.

(E) Purification of endogenous MK2 isoforms from RAW264.7 cells. Endogenous MK2 was purified from 1 × 10^8 RAW264.7 cells using a MK2-Trap. Lysate, flowthrough, and precipitates were separated by SDS-PAGE. Bands were excised for mass spectrometry.

(F) Identification of MK2 peptides from mass spectrometry. The three translation initiation sites are marked in bold and italics. Red sequences depict detected peptides, and black sequences depict non-detected ones.

See also Figures S1, S2, S3, and S4.

observe such footprints in murine and human cell lines in the 5′ UTR of MK2 (Figures S3 and S4).

To validate the existence of an N-terminal extended MK2, we purified endogenous MK2 from murine RAW264.7 cells that express almost equal levels of both MK2 isoforms (Figures 1A and 1E). By using a MK2-Nanotrap, we were able to enrich and purify considerable amounts of endogenous MK2 from these cells and subsequently analyzed them by mass spectrometry (Figures 1E and 1F). We readily identified peptides derived from the predicted in-frame 5′ UTR extension originating from the CUG alternative translation initiation sites at position −141 (Figure 1F). The detection of peptides derived from sequences further upstream of this CUG indicates that the GUG in position −309 or other codons may also be used for alternative translation initiation. In sum, these results confirmed the existence of at least one alternative translation initiation site at position −141 in the 5′ UTR of the MK2 transcript, resulting in the translation of a minimum of two distinct MK2 isoforms in murine and human cells from the same mRNA.

Mechanistic Insights into Regulation of MK2 Translation

To further characterize the usage of the putative alternative translation initiation site at position −141 of MK2 mRNA, we fused the extended endogenous murine 5′ UTR with the known murine MK2 ORF and expressed the construct in different cell lines. The high GC content of the 5′ UTR (>85%) prompted us to introduce a synthetic DNA flanked by restriction sites (Figure S5A). Expression of the 5′ UTR-MK2-ORF construct resulted in the two-band pattern known for endogenous murine MK2 (Figures 2A, S5B, and S5C). Mutagenesis of the putative alternative translation initiation sites at positions −141 and −309 resulted in an altered band pattern and revealed that the triplet CUG at −141 is used for alternative translation initiation under these conditions, leading to expression of the long isoform (Figure 2A, lane 5). Nonetheless, the CUG is a much weaker initiation site than AUG (Figures 2A; compare lanes 2, 3, and 4). Disrupting the alternative Kozak sequence surrounding the CUG (adjacent GAG to CAU) impaired the expression of the long isoform (Figure 2A, lane 6). Interestingly, it was even possible to generate a super-long MK2 isoform by mutating −309 GUG to AUG (Figure 2A, lane 7).

Next, we explored the underlying molecular mechanism allowing MK2 isoform translation *in vivo*. Human cells treated with the anti-cancer drug silvestrol (also known as rocaglamide) respond with a decrease in the translation of a selective set of mRNAs due to inhibition of the RNA helicase eIF4A1 (Modelska et al., 2015; Wolfe et al., 2014). Among them, MK2 mRNA is a major target (Wolfe et al., 2014). Additionally, it was suggested that mRNAs commonly regulated by this mechanism contain long and GC-rich 5′ UTRs with potential G-rich quadruplex structures (Modelska et al., 2015; Wolfe et al., 2014). In turn, recent data show that eIF4A1 is rather clamped to purine-rich, motif-containing transcripts by rocaglamide, inhibiting their translation and questioning the requirement of eIF4A1 in G-rich quadruplex structure resolution (Iwasaki et al., 2016; Iwasaki et al., 2019). Furthermore, it was shown that eIF4A1 targets preferentially mRNAs with 5′ UTRs containing classical secondary structures rather than G-quadruplexes (Waldron et al., 2018). Nonetheless, and due to the high GC content of MK2's 5′ UTR, we were able to detect computationally predicted sequences (Kikin et al., 2006) that could give rise to G-rich quadruplex structures located upstream of the alternative translation initiation site CUG and the AUG within the 5′ UTR of human and murine MK2 (Table S1). Independent of the existence of these structures, we speculated that the helicase eIF4A1 might play a role in general or selective MK2 isoform translation. As seen, upon depletion of eIF4A1, a marked decrease in translation of both MK2 isoforms in murine cells and, at least, a decrease of the short isoform in human cells were observed (Figures 2B and S6A). It was proposed that the translation initiation auxiliary factor eIF2A is important for non-AUG translation initiation (summarized in Kearse and Wilusz, 2017) and expression of the PTEN isoform PTEN-alpha has been described to be dependent on this factor and a surrounding palindromic sequence (Hopkins et al., 2013; Liang et al., 2014). However, we only observed non-selective moderate effects of eIF2A depletion on MK2 translation in murine cells (Figure 2B). In contrast to the literature, we detected a stronger dependence of the PTEN/PTEN-alpha translation on eIF4A1, as small interfering RNA (siRNA)-mediated depletion of eIF2A interfered with eIF4A1 downregulation (Figure 2B, lane 3). Possibly due to insufficient siRNA-mediated depletion, we could not detect any effects of eIF2A on human PTEN/PTEN-alpha level (Figure S6A). We then re-analyzed the mouse organs (Figure 1B) for eIF4A1 expression (Figure 2C). Higher eIF4A1 levels principally correlated with higher levels of both MK2 isoforms, but it remains too tempting to postulate a final conclusion at this stage.

Epigenetic markers of mRNAs, such as m^6-adenosine methylation, influence the stability and translation of modified mRNAs (Fu et al., 2014). Human MK2 mRNA is heavily methylated near the stop codon, and translation of MK2 mRNA was reported to be strongly decreased upon depletion of the methyltransferase METTL3 (Lin et al., 2016; Wang et al., 2015). However, we could only observe a moderate decrease of MK2 protein in HEK293T, which was accompanied by a known METTL3-dependent decrease in SRF protein level (Müller et al., 2018) (Figure S6B). We were not able to get conclusive results from Mettl3 knockdown experiments in murine cells and do not know whether murine MK2 mRNA undergoes methylation *in vivo* (Figure S6B).

To additionally prove a role for the GC-rich sequences in MK2 isoform translation, we generated a set of MK2 reporter mutants that were intended to recapitulate the requirement of these sequences for the translation of the long alternative MK2 isoform (Figure 2D, left): compared to the 5′ UTR full-length construct (1), the sequences upstream of the alternative translation initiation site CUG were either completely truncated (2) or replaced by an unstructured short beta-globin stretch (3), a combination of beta-globin with scrambled GC-rich sequences (4), or beta-globin fused to GC-rich sequences known to form three-layered G-quadruplex sequences and known to inhibit translation (5). Clearly, the loss of CUG upstream sequences abrogated translation of the long MK2 isoform, as compared to the full-length construct (Figure 2D, lanes 1 and 2). Stepwise rescue of GC-rich sequences enhances long isoform translation (Figure 2D, lanes 3 and 4), whereas true G-rich quadruplexes inhibited markedly long and importantly also short isoform translation (Figure 2D, lane 5). This supported the notion that GC-rich

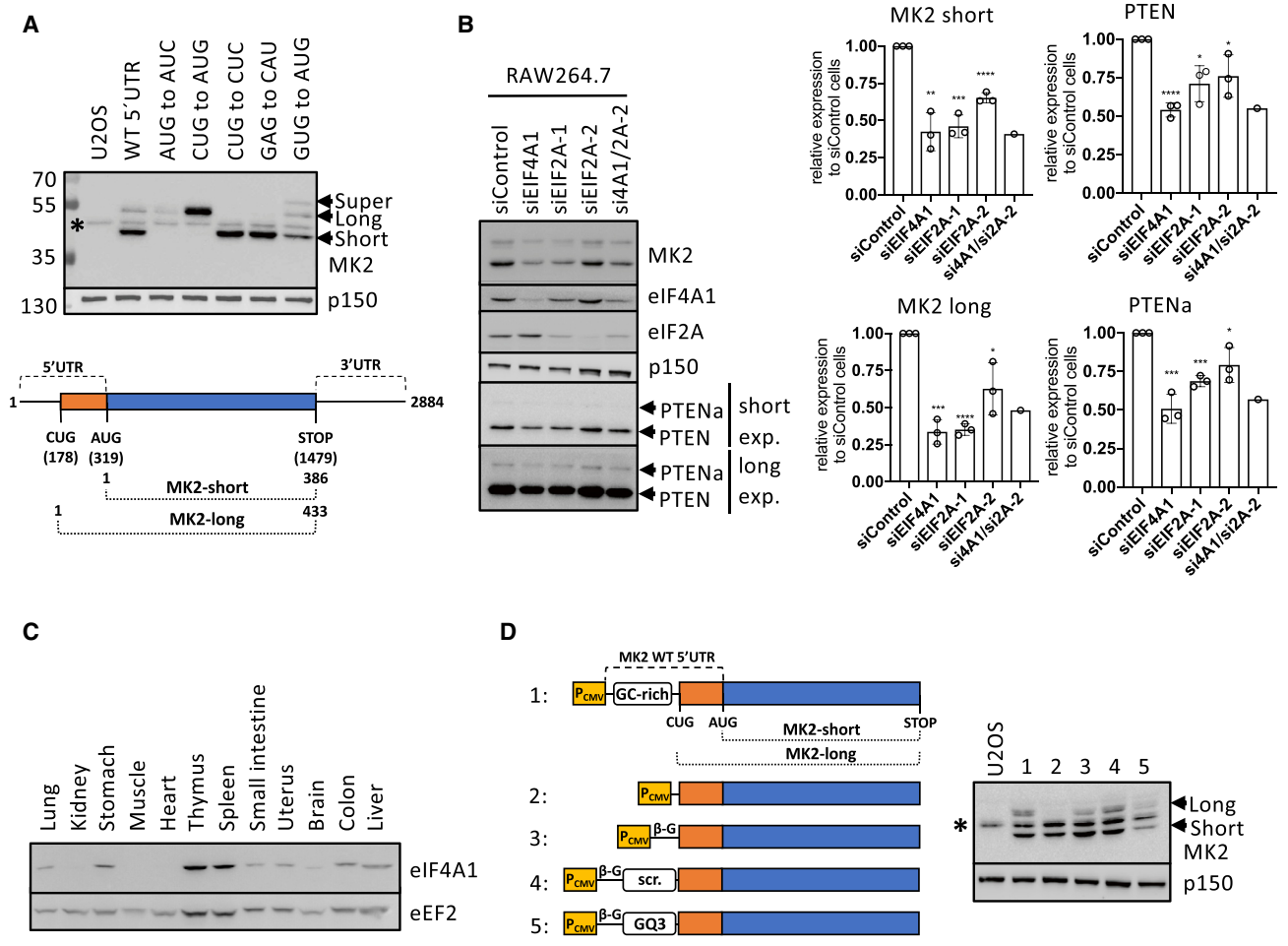

Figure 2. Mechanistic Insights into Regulation of MK2 Translation

(A) Expression of murine MK2 5′ UTR isoforms in U2OS cells through the introduction of 5′ UTR point mutations (see Figure S5A). Lysates were analyzed by western blot with an anti-MK2 antibody and an anti-p150 antibody as loading controls. Arrows indicate the different MK2 isoforms. The resulting schematic representation of codon usage and their consequent translation into the short and long MK2 isoforms is shown below.

(B) RAW264.7 cells were transfected with siRNAs targeting eIF4A1 or eIF2A. Lysates were analyzed for eIF4A1 and eIF2A levels to monitor knockdown efficacy and MK2 and PTEN to detect consequences of the knockdowns. p150 was used to normalize the signals for quantification. Three biological replicates (n = 3) were performed and used for quantifications of the signals (except for the double knockdown of eIF4A1 and eIF2A [n = 1]) and are shown as means ± SD. Arrows indicate PTEN and its longer isoform PTEN-alpha. *p ≤ 0.05; **p ≤ 0.01; ***p ≤ 0.001; ****p ≤ 0.0001.

(C) Reanalysis of the mouse organ lysates from Figure 1B to test for eIF4A1 expression. Loading control: eEF2.

(D) Schematic representation of MK2 reporter constructs (1–5) to analyze the role of GC-rich sequences in CUG usage (left). β-G, beta-globin; scr., scrambled GC rich; GQ3, three-layered G-rich quadruplex. The asterisk indicates the endogenous short MK2 isoform from U2OS cells. p150 was used as loading control.

See also Figures S5 and S6 and Table S1.

sequences forming classical secondary structures rather than G-rich quadruplexes promote translation of the long MK2 isoform. In summary, we demonstrate a major role for the RNA helicase eIF4A1 in the translation of distinct MK2 isoforms and suggest that GC-rich sequences upstream of the alternative translation initiation site CUG support long isoform translation from a single mRNA species (Figure S6C).

Functional Characterization of MK2 Isoforms

To address the physiological consequences of MK2 isoform expression, we stably reconstituted MK2-deficient mouse embryonic fibroblast (MEF) cell lines (Ronkina et al., 2007) with the short, the long, or both isoforms of MK2 expressed to similar levels, as compared to endogenous MK2 in RAW264.7 and HEK293T cells (Figure 3A). Interestingly, when using the super-long isoform for rescuing the MK2-deficient MEFs (Figure S7A), we lost the expression of all other MK2 isoforms observed in transient transfection experiments (cf. Figures 2A, S5B, and S5C). First, we assessed the relative stability of the two MK2 isoforms after a cycloheximide-induced block of *de novo* protein translation in the rescued cells in comparison to the endogenous isoforms in RAW264.7 and HEK293T cells (Figures 3B, 3C and S7B). As seen, the longer variant was considerably more stable than the short isoform in these assays. Nuclear cytosolic

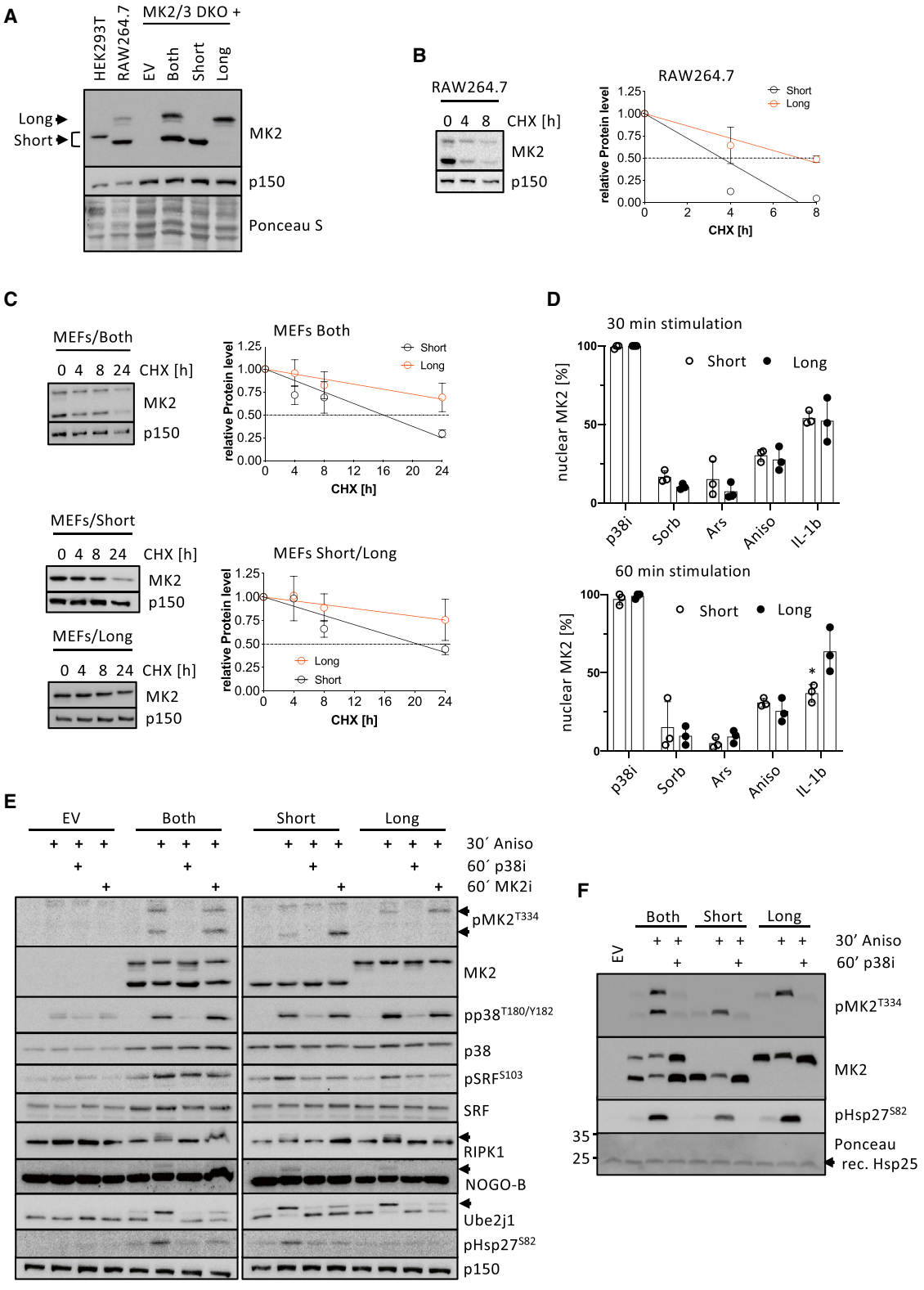

Figure 3. Functional Characterization of MK2 Isoforms

(A) Complementation of MK2/3 DKO mouse embryonic fibroblasts (MEFs) by retroviral transduction with MK2 constructs derived from Figure 2A. Empty-vector-transduced cells served as controls. Isoform expression levels are compared to the expression of endogenous MK2 isoforms in RAW264.7 and HEK293T cells.

(legend continued on next page)

shuttling of MK2 triggered by activated $p38^{MAPK}$ is a hallmark of MK2 activation (summarized in Gaestel, 2006). We, therefore, compared the localization of both isoforms in non-stressed cells, and, when we activated $p38^{MAPK}$ by different stresses, their redistribution over time to the cytosol (Figures 3D and S7C). Regardless of the stress conditions, no substantial differences of the isoforms in shuttling from the nucleus to cytosol were observed. Monitoring the redistribution of the super-long isoform was not possible, since transfection of this construct was accompanied by short and long isoform expression (Figure S7D). We then tested the ability of the isoforms in cells to phosphorylate the known MK2 substrates Ube2j1, SRF, RIPK1, Reticulon 4B/NOGO-B, and Hsp27 (also HSBP1 or Hsp25 in mice) upon activation by anisomycin in a $p38^{MAPK}$-dependent manner (Figure 3E). The specificity of phosphorylation was assessed with chemical inhibitors against MK2's upstream kinase $p38^{MAPK}$ (p38i) and MK2 itself (MK2i) (Figure 3E). In accordance with previous reports (Ronkina et al., 2007), we also detected reduced total $p38^{MAPK}$ level in MK2/3 double-deficient cells (see empty vector (EV)-transduced cells). While substrates were readily phosphorylated by both isoforms, phosphorylation of the small heat shock protein Hsp27, a bona fide substrate of MK2, could only be detected for the short MK2 isoform (Figure 3E). This finding indicated the intriguing possibility that both isoforms differed in their substrate specificity *in vivo*. To further test this, we performed an *in vitro* kinase assays using purified MK2 isoforms from rescued MEFs and recombinant murine Hsp25 (Figures 3F and S7E). We could not confirm the inability of the long MK2 isoform to phosphorylate Hsp25 under these conditions, indicating the existence of a ternary factor, which inhibits long MK2-Hsp27 interaction *in vivo*. Taken together, we were able to reconstitute MK2-deficient cells with individual isoforms. Both murine isoforms of MK2 share molecular properties, such as the ability to translocate from the nucleus to the cytoplasm, but differ in their stability and probably in their substrate specificity *in vivo*.

Phenotypical Consequences of MK2 Isoform Expression

Expression of both isoforms differs among mouse tissues (Figure 1B). Therefore, we speculated on physiologically relevant differences and attempted to explore the phenotypical consequences of isoform expression in MK2/3-deficient MEFs. We initially tested proliferation of the differently rescued cell lines (Figure S8A). Cells grew to a similar extent independently of the isoform used for rescue. We then checked the induction of the immediate early genes (IEGs) early growth response 1 (Egr1), FBJ osteosarcoma oncogene (cFos), and TTP (or Zfp36) upon anisomycin stimulation of MK2/3-deficient MEFs rescued with the different isoforms of MK2 (Figure 4A). While expression of the short isoform elevated the expression of all of these genes, the long isoform of MK2 was not able to induce IEGs. Of note, we were not able to detect differences in SRF phosphorylation by the isoforms (Figure 3E), indicating that other MK2-dependent mechanisms regulate IEG transcription under these conditions. Since it is known that the N terminus of MK2 plays an important role in cell motility (Kotlyarov et al., 2002), we also assayed for cell migration using a scratch assay (Figure 4B). As seen, the migration phenotype could only be rescued by the short MK2 isoform, consistent with our observation that only the short isoform of MK2 is competent for phosphorylation of the migration-associated substrate Hsp27 (Figure 3E). Collectively, these results highlighted differential functional properties of MK2 isoforms.

MK2 Isoform Interaction Profiling

The phenotypic differences in our rescue cell lines suggested that the two MK2 isoforms could have overlapping and unique interaction partners. As a control for the proficiency of both proteins, we first precipitated the isoforms with MK2-Trap beads and confirmed their well-characterized interaction with the upstream activating kinase $p38^{MAPK}$ (Figure S8B). We then used quantitative mass spectrometry to analyze the interaction partners of both isoforms in cells that were left untreated or treated with combinations of anisomycin and the MK2 inhibitor (MK2i) PF-3644022. This approach allowed us to compare MK2 activity-dependent interaction partners of the two MK2 isoforms. While we detected only a few isoform-specific interactions in resting cells (i.e., Polr1b for the long isoform), stress induction by anisomycin, especially in combination with the MK2 inhibitor, revealed a strong bias toward the short MK2 isoform for

(B) The stability of MK2 isoforms in RAW264.7 cells was analyzed after cycloheximide (CHX) chase for the indicated times. The p150 loading control was used to normalize MK2 signals. Three independent biological replicates (n = 3) were analyzed for each sample, and the mean of them ± SD is shown for each time point. The blots show representative results of one replicate.

(C) The stability of MK2 isoforms in MK2/3 DKO complemented MEFs was analyzed after chasing cells with cycloheximide (CHX) for the indicated times. The p150 loading control was used to normalize MK2 signals. Three independent biological replicates (n = 3) were analyzed for each sample, and the mean of them ± SD is shown for each time point. The blots show a representative result of one replicate.

(D) Fluorescence microscopy to determine the percentage of nuclear and cytosolic MK2 after treatment with $p38^{MAPK}$ activators. The results show the mean of three independent biological replicates (n = 3) ± SD. For each replicate, a minimum of 100 cells were counted. Cells incubated with a p38 inhibitor (p38i) served as a negative control. *$p \leq 0.05$ (unpaired t test).

(E) Complemented MK2/3 DKO MEFs were analyzed for MK2 substrate phosphorylation upon anisomycin stimulation. Phosphorylation of $p38^{MAPK}$ ($pp38^{T180/Y182}$) and MK2 ($pMK2^{T334}$) itself was used as a readout for activation of the pathway. To control activity and selectivity of MK2 substrate phosphorylations, cells were either pre-incubated with a $p38^{MAPK}$ inhibitor (p38i) or an MK2 inhibitor (MK2i). Loading control: p150. In the case of RIPK1, NOGO-B and Ube2j1 protein shifts (indicated by arrows) were used as readouts.

(F) Semi *in vitro* non-radioactive kinase assay. MK2 isoforms were purified from MEFs after the indicated treatments. Precipitates were incubated with 600 ng recombinant murine Hsp25 in the presence of ATP. Phosphorylation of Hsp25 was tested by western blot using a phospho-specific anti-$pHsp27^{S82}$ antibody. A phospho-specific anti-$pMK2^{T334}$ was used to monitor MK2 activation. Specificity was confirmed by the $p38^{MAPK}$ inhibitor (p38i) samples. Ponceau staining of the membrane showed equal presence of recombinant murine Hsp25 in all samples.

See also Figure S7.

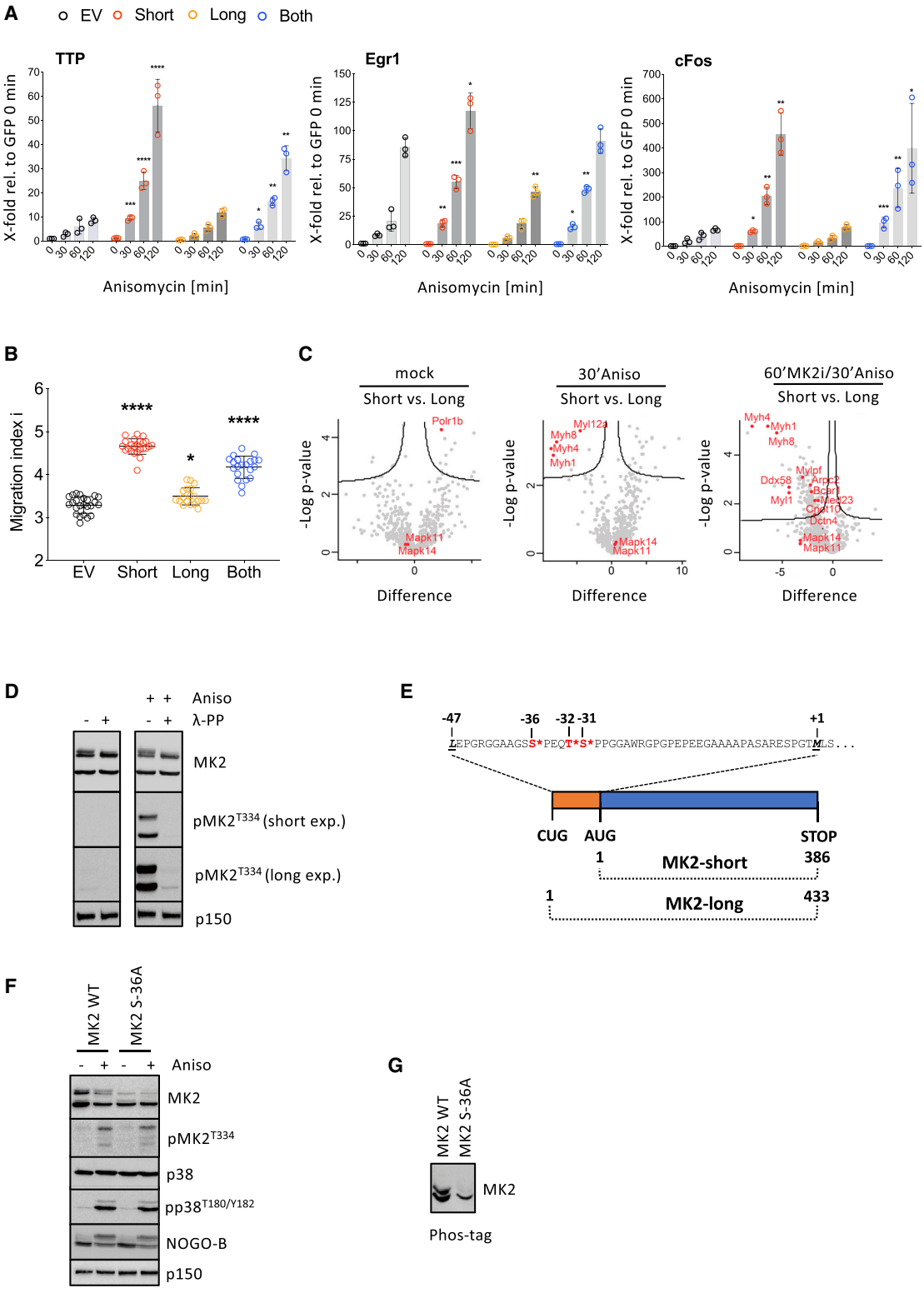

Figure 4. Consequences of MK2 Isoform Expression

(A) Analysis of TTP, cFos, and Egr1 expression upon anisomycin stimulation in rescued MEFs. Each data point represents a biological replicate that was measured in duplicates. Error bars represent the mean of three independent replicates (n = 3) ± SD. The p values were retrieved from unpaired t tests using PRISM 8 software and are related to GFP/EV-rescued MEFs. *p ≤ 0.05; **p ≤ 0.01; ***p ≤ 0.001; ****p ≤ 0.0001.

(legend continued on next page)

interaction with proteins of the myosin family (Myh1, Myh4, Myh8, Myl1, Myl12a, and and Mylpf) and the transcriptional machinery (Med23 and Cnot10) (Figure 4C; Data S2). Gene Ontology (GO) term analysis (Figure S8C) revealed proteins, such as Arpc2 or Ddx58, to interact with the short MK2 isoform (Figure 4C), connecting it to the cytoskeleton via actin or the myosin machinery. Given the fact that MK2-dependent migration is only rescued by the short isoform, which is also uniquely capable of phosphorylating Hsp27 upon stress *in vivo* (Figure 3E), we speculate that these short-isoform-specific interactions underlie the migration of MK2-proficient cells. In line with our biochemical experiment (Figure 3E), our proteomics analysis confirmed that both MK2 isoforms readily interact with p38alpha/beta (Mapk11/14) in a stimulus-independent manner (Figure 4C; Figure S8B). Furthermore, we were able to confirm the interaction of the long isoform with Polr1b under resting conditions (Figure S8D). Surprisingly, we were not able to detect this interaction when both isoforms were co-expressed (Figure S8D). Attempts to validate specific interaction of the short isoform with proteins of the myosin family by western blot failed due to the lack of specific antibodies.

When we strongly overexpressed MK2 in HEK293T or HeLa cells, we detected a double-band pattern of the long isoform indicating, e.g., phosphorylation events in the extended N terminus of long MK2 (cf. Figures S5B and S5C). Consequently, the upper of the two bands disappeared when treating lysates with lambda-phosphatase (Figure 4D). Importantly, the double-band pattern was not a result of stress-induced MK2 phosphorylation (Figure 4D). Since we enriched the MK2 isoforms for our interaction profiling approach, it was possible to detect unique long-isoform-specific, proline-directed serine and threonine phosphorylation sites in the extended N terminus in the mass spectrometry analysis (Figure 4E). Introducing point mutations in the extended N terminus revealed serine −36, relative to the canonical initiating methionine, to be constitutively phosphorylated, as its mutation to alanine resulted in an almost complete loss of the double-band pattern without changing the phosphorylation status of MK2 at the known T334 site (T320 in mouse) (Figure 4F). Re-analyzing the same type of samples on a Phos-tag gel confirmed this observation (Figure 4G) and supported the idea of an additional constitutive serine phosphorylation in the unique N terminus of long MK2. Attempts to identify the kinase targeting this site *in vivo* were difficult, as the target site seems not be stress regulated, and the sequences surrounding serine-36 display no classical proline-directed motif.

Taken together, these results revealed that the two MK2 isoforms have both common and distinct interaction partners. The specific interactions of the short isoform with migration-associated proteins and transcriptional regulators may explain why some MK2-dependent phenotypes are only rescued by this MK2 variant. On the other hand, the unique N terminus of the long isoform displays at least one serine that is constitutively phosphorylated by a yet-unidentified kinase.

DISCUSSION

An N-terminal extended long isoform of the protein kinase MK2 is constitutively translated from an in-frame CUG alternative translation initiation site upstream of the known AUG initiation codon. The constitutive usage of this alternative translation initiation site was confirmed by mutational studies and analyses of ribosome footprinting data. These findings were supported by the detection of endogenous peptides by mass spectrometry.

Two reports identified MK2 as a target of the RNA helicase eIF4A1 (Modelska et al., 2015; Wolfe et al., 2014). Our data show that eIF4A1 regulates MK2 translation of both isoforms. By using MK2 5′ UTR reporter constructs, we could exclude that the usage of CUG is supported by potential surrounding G-quadruplex structures that are usually known to negatively regulate translation (Bugaut and Balasubramanian, 2012). In turn, rather classical, secondary structured GC-rich sequences sensitive to eIF4A1 (Waldron et al., 2018) upstream of the CUG support its usage as an initiation site. The data suggested that the scanning mechanism of the ribosome is slowed down, and, consequently, a leaky scanning leads to the usage of the CUG for translation initiation. This mechanism appears evolutionarily conserved, yet murine cells produce relatively more of the long and alternative isoforms compared to their human counterparts. This correlates with the fact that the human 5′ UTR is shorter than that of the murine counterpart and that the GC-rich sequences surrounding the CUG are shorter.

Examples of in-frame N-terminal protein extensions originating from alternative translation starting in the 5′ UTR have previously been described, i.e., for PTEN (Hopkins et al., 2013; Liang et al., 2014) or thioredoxin/glutathione (Gerashchenko et al., 2010). It was suggested that eIF2A is a specificity factor for non-AUG translation initiation (summarized in Kearse and Wilusz, 2017). To this end, we only observed moderate effects of eIF2A on MK2 translation. It also remains to be clarified whether the RNA helicase Ddx3 (Guenther et al., 2018) is a regulatory

(B) Fluorescence-based scratch wound healing assay for rescued MEFs. Each individual data point represents a biological replicate ($n \geq 19$), and the mean of all replicates is shown ± SD. The p values were retrieved from an ordinary one-way ANOVA using PRISM 8 software and are related to EV-transduced MK2-deficient MEFs. *$p \leq 0.05$; ****$p \leq 0.0001$.

(C) Volcano plots of significantly short- and long-isoform-interacting proteins at the indicated conditions. Selected proteins are highlighted in red. The black lines define the border of significantly interacting proteins. Significance was calculated in MaxQuant.

(D) Transfection of HEK293T cells with a 5′ UTR-MK2 wild-type construct. Samples were treated as indicated and analyzed for phosphatase-sensitive bands by western blots. Blotting for phosphorylated MK2 ($pMK2^{T334}$) served as dephosphorylation control (right). Loading control: p150.

(E) Schematic representation of long-isoform-specific unique phosphorylated residues within the extended N terminus. Phosphorylated residues are highlighted in red with a star and are numbered in relation to the initiating methionine of the canonical MK2 ORF.

(F) Expression of 5′ UTR-MK2 wild-type or S-36A-5′ UTR-MK2 mutant in HEK293T cells. Treatment as indicated. Blots against phosphorylated $p38^{MAPK}$ and NOGO-B served as controls for activation by anisomycin. Loading control: p150.

(G) The indicated samples from transfected HEK293T cells were analyzed with a Phos-tag gel.

See also Figure S8.

factor for MK2 isoform translation alone or in cooperation with eIF4A (Gao et al., 2016).

The long MK2 isoform identified here behaves in a manner identical to that of the canonical protein in terms of activation by and interaction with the upstream kinase $p38^{MAPK}$. On the other side, the long MK2 isoform had a decreased turnover rate as compared to its short counterpart, displayed a unique additional serine phosphorylation site in its extended N terminus, and failed to phosphorylate the MK2 bona fide substrate Hsp27 upon anisomycin stimulation *in vivo* (summarized in Figure S8E). This is similar to the different $p38^{MAPK}$ isoforms, which exhibit distinct substrate specificities although displaying a high degree of amino-acid sequence identity (Cuenda and Rousseau, 2007). In an MK2-deficient background, only expression of the short MK2 isoform or both isoforms can rescue migration and IEG defects. As revealed by mass spectrometry, the preferred binding of the short MK2 isoform to proteins of the cytoskeleton and the transcription machinery correlates with the unique ability of this isoform to rescue migration and transcriptional defects. Both processes are well-established MK2-dependent responses (Menon et al., 2009; Ronkina et al., 2011). The long isoform of MK2 is likely to have exclusive functions as well. The unique N-terminal extension of this protein contains putative proline-directed serine and threonine phosphorylation sites. We could determine S-36 to be constitutively phosphorylated by a yet-unidentified kinase. Interestingly, the phosphorylation of this site is not induced by stress activation. We, therefore, speculate that this site is targeted by other proline-directed kinases than $p38^{MAPK}$, such as cyclin-dependent kinases (CDKs) (Malumbres, 2014). Isoform-specific modifications could potentially allow for the recruitment of unique substrates and the assignment of unique functions of the long MK2 isoform and clearly warrant future investigation. We can only speculate on the consequences of this phosphorylation, but we want to stress that expression of the short isoform alone was often accompanied by a "super-rescue" of MK2 deficiency, compared to the rescue by expression of both isoforms together (see Figures 4A and 4B). Furthermore, using IUPred2A (Mészáros et al., 2018) showed that the extended N terminus is entirely disordered. Nonetheless, the long isoform failed to localize to stress granules or P-bodies (data not shown).

Future phospho-proteomic studies could shed additional light on the substrate specificities of the two MK2 isoforms and their relevance *in vivo*. Our work reveals the abundant translation of a hitherto unrecognized MK2 isoform with unique functional properties, highlighting that the biology of this kinase is still not fully understood. Our work also resolves a long-standing mystery surrounding the presence of the additional high-molecular-weight MK2 band (Cano et al., 1996; Ronkina et al., 2007; Stokoe et al., 1992).

STAR★METHODS

Detailed methods are provided in the online version of this paper and include the following:

- KEY RESOURCES TABLE
- CONTACT FOR REAGENT AND RESOURCE SHARING
- EXPERIMENTAL MODEL AND SUBJECT DETAILS
- METHOD DETAILS
  - Tissue culture, cell lines, treatments
  - Isolation of mouse organs/bone marrow-derived macrophages
  - Transfection of cell lines
  - siRNA transfections
  - Generation of stable shRNA knockdown cell lines
  - Cloning
  - SDS-PAGE and Western Blot
  - Protein dephosphorylation assay
  - Kinase Assay
  - MK2 precipitation and LC-MS for the identification of MK2 peptides
  - MK2 interaction profiling by label-free mass-spectrometry
  - Migration Assay
  - WST-1 Assay
  - RNA extraction and qPCR
  - Microscopy
  - Bioinformatic analyses
- QUANTIFICATION AND STATISTICAL ANALYSIS
- DATA AND SOFTWARE AVAILABILITY

SUPPLEMENTAL INFORMATION

Supplemental Information can be found online at https://doi.org/10.1016/j.celrep.2019.05.024.

ACKNOWLEDGMENTS

The following people and institutions are thanked for providing expertise and reagents: Dr. Mathias Ballmaier and the sorting facility of the Hannover Medical School and Prof. Andreas Pich and the mass spectrometry facility at the Hannover Medical School for performing initial mass spectrometry to identify isoforms. C.T. thanks Katrin Laaß for excellent technical assistance. This work was founded by grants from the Lundbeck fonden and the NEYE Fonden. M.D.D.-M. and M.T. were funded by the "Biotechnology and Biological Sciences Research Council (BBSRC)." M.G. was funded by the Deutsche Forschungsgemeinschaft.

AUTHOR CONTRIBUTIONS

P.T. and G.S. performed the majority of the experiments; M.B.M. and R.F. performed experiments; D.B.-J. and J.V.O. performed mass spectrometry experiments and the analyses; M.D.D.-M. performed bioinformatics analyses; M.G. and C.T. identified the odd reads in the 5′ UTR of the MK2 gene; A.K. designed experiments; M.T., M.G., and S.B.-J. supervised the study, provided lab space, and contributed to the writing of the manuscript; and C.T. performed experiments and wrote the paper. All authors read and contributed to the editing of the final manuscript.

DECLARATION OF INTERESTS

The authors declare no competing interests.

Received: October 29, 2018
Revised: April 10, 2019
Accepted: May 6, 2019
Published: June 4, 2019

REFERENCES

Afgan, E., Baker, D., van den Beek, M., Blankenberg, D., Bouvier, D., Čech, M., Chilton, J., Clements, D., Coraor, N., Eberhard, C., et al. (2016). The Galaxy platform for accessible, reproducible and collaborative biomedical analyses: 2016 update. Nucleic Acids Res. *44* (*W1*), W3–W10.

Barbosa, C., Peixeiro, I., and Romão, L. (2013). Gene expression regulation by upstream open reading frames and human disease. PLoS Genet. *9*, e1003529.

Bekker-Jensen, D.B., Kelstrup, C.D., Batth, T.S., Larsen, S.C., Haldrup, C., Bramsen, J.B., Sorensen, K.D., Hoyer, S., Orntoft, T.F., Andersen, C.L., et al. (2017). An optimized shotgun strategy for the rapid generation of comprehensive human proteomes. Cell Syst. *4*, 587–599.e4.

Blasius, M., Wagner, S.A., Choudhary, C., Bartek, J., and Jackson, S.P. (2014). A quantitative 14-3-3 interaction screen connects the nuclear exosome targeting complex to the DNA damage response. Genes Dev. *28*, 1977–1982.

Bugaut, A., and Balasubramanian, S. (2012). 5′-UTR RNA G-quadruplexes: translation regulation and targeting. Nucleic Acids Res. *40*, 4727–4741.

Cano, E., Doza, Y.N., Ben-Levy, R., Cohen, P., and Mahadevan, L.C. (1996). Identification of anisomycin-activated kinases p45 and p55 in murine cells as MAPKAP kinase-2. Oncogene *12*, 805–812.

Cox, J., Hein, M.Y., Luber, C.A., Paron, I., Nagaraj, N., and Mann, M. (2014). Accurate proteome-wide label-free quantification by delayed normalization and maximal peptide ratio extraction, termed MaxLFQ. Mol. Cell. Proteomics *13*, 2513–2526.

Cuenda, A., and Rousseau, S. (2007). p38 MAP-kinases pathway regulation, function and role in human diseases. Biochim. Biophys. Acta *1773*, 1358–1375.

Dondelinger, Y., Delanghe, T., Rojas-Rivera, D., Priem, D., Delvaeye, T., Bruggeman, I., Van Herreweghe, F., Vandenabeele, P., and Bertrand, M.J.M. (2017). MK2 phosphorylation of RIPK1 regulates TNF-mediated cell death. Nat. Cell Biol. *19*, 1237–1247.

Fields, A.P., Rodriguez, E.H., Jovanovic, M., Stern-Ginossar, N., Haas, B.J., Mertins, P., Raychowdhury, R., Hacohen, N., Carr, S.A., Ingolia, N.T., et al. (2015). A regression-based analysis of ribosome-profiling data reveals a conserved complexity to mammalian translation. Mol. Cell *60*, 816–827.

Fijalkowska, D., Verbruggen, S., Ndah, E., Jonckheere, V., Menschaert, G., and Van Damme, P. (2017). eIF1 modulates the recognition of suboptimal translation initiation sites and steers gene expression via uORFs. Nucleic Acids Res. *45*, 7997–8013.

Fritsch, C., Herrmann, A., Nothnagel, M., Szafranski, K., Huse, K., Schumann, F., Schreiber, S., Platzer, M., Krawczak, M., Hampe, J., and Brosch, M. (2012). Genome-wide search for novel human uORFs and N-terminal protein extensions using ribosomal footprinting. Genome Res. *22*, 2208–2218.

Fu, Y., Dominissini, D., Rechavi, G., and He, C. (2014). Gene expression regulation mediated through reversible m^6A RNA methylation. Nat. Rev. Genet. *15*, 293–306.

Gaestel, M. (2006). MAPKAP kinases - MKs - two's company, three's a crowd. Nat. Rev. Mol. Cell Biol. *7*, 120–130.

Gaestel, M. (2013). What goes up must come down: molecular basis of MAPKAP kinase 2/3-dependent regulation of the inflammatory response and its inhibition. Biol. Chem. *394*, 1301–1315.

Gao, Z., Putnam, A.A., Bowers, H.A., Guenther, U.P., Ye, X., Kindsfather, A., Hilliker, A.K., and Jankowsky, E. (2016). Coupling between the DEAD-box RNA helicases Ded1p and eIF4A. eLife *5*, e16408.

Gawron, D., Ndah, E., Gevaert, K., and Van Damme, P. (2016). Positional proteomics reveals differences in N-terminal proteoform stability. Mol. Syst. Biol. *12*, 858.

Gerashchenko, M.V., Su, D., and Gladyshev, V.N. (2010). CUG start codon generates thioredoxin/glutathione reductase isoforms in mouse testes. J. Biol. Chem. *285*, 4595–4602.

Guenther, U.P., Weinberg, D.E., Zubradt, M.M., Tedeschi, F.A., Stawicki, B.N., Zagore, L.L., Brar, G.A., Licatalosi, D.D., Bartel, D.P., Weissman, J.S., and Jankowsky, E. (2018). The helicase Ded1p controls use of near-cognate translation initiation codons in 5′ UTRs. Nature *559*, 130–134.

Hinnebusch, A.G., Ivanov, I.P., and Sonenberg, N. (2016). Translational control by 5′-untranslated regions of eukaryotic mRNAs. Science *352*, 1413–1416.

Hoffman, L., Jensen, C.C., Yoshigi, M., and Beckerle, M. (2017). Mechanical signals activate p38 MAPK pathway-dependent reinforcement of actin via mechanosensitive HspB1. Mol. Biol. Cell *28*, 2661–2675.

Hopkins, B.D., Fine, B., Steinbach, N., Dendy, M., Rapp, Z., Shaw, J., Pappas, K., Yu, J.S., Hodakoski, C., Mense, S., et al. (2013). A secreted PTEN phosphatase that enters cells to alter signaling and survival. Science *341*, 399–402.

Ingolia, N.T., Lareau, L.F., and Weissman, J.S. (2011). Ribosome profiling of mouse embryonic stem cells reveals the complexity and dynamics of mammalian proteomes. Cell *147*, 789–802.

Ingolia, N.T., Brar, G.A., Rouskin, S., McGeachy, A.M., and Weissman, J.S. (2012). The ribosome profiling strategy for monitoring translation in vivo by deep sequencing of ribosome-protected mRNA fragments. Nat. Protoc. *7*, 1534–1550.

Iwasaki, S., Floor, S.N., and Ingolia, N.T. (2016). Rocaglates convert DEAD-box protein eIF4A into a sequence-selective translational repressor. Nature *534*, 558–561.

Iwasaki, S., Iwasaki, W., Takahashi, M., Sakamoto, A., Watanabe, C., Shichino, Y., Floor, S.N., Fujiwara, K., Mito, M., Dodo, K., et al. (2019). The translation inhibitor rocaglamide targets a bimolecular cavity between eIF4A and polypurine RNA. Mol. Cell *73*, 738–748.e9.

Jaco, I., Annibaldi, A., Lalaoui, N., Wilson, R., Tenev, T., Laurien, L., Kim, C., Jamal, K., Wicky John, S., Liccardi, G., et al. (2017). MK2 phosphorylates RIPK1 to prevent TNF-induced cell death. Mol. Cell *66*, 698–710.e5.

Jensen, O.N., Wilm, M., Shevchenko, A., and Mann, M. (1999). Sample preparation methods for mass spectrometric peptide mapping directly from 2-DE gels. Methods Mol. Biol. *112*, 513–530.

Jochim, N., Gerhard, R., Just, I., and Pich, A. (2011). Impact of clostridial glucosylating toxins on the proteome of colonic cells determined by isotope-coded protein labeling and LC-MALDI. Proteome Sci. *9*, 48.

Kearse, M.G., and Wilusz, J.E. (2017). Non-AUG translation: a new start for protein synthesis in eukaryotes. Genes Dev. *31*, 1717–1731.

Kikin, O., D'Antonio, L., and Bagga, P.S. (2006). QGRS Mapper: a web-based server for predicting G-quadruplexes in nucleotide sequences. Nucleic Acids Res. *34*, W676–W682.

Kotlyarov, A., Neininger, A., Schubert, C., Eckert, R., Birchmeier, C., Volk, H.D., and Gaestel, M. (1999). MAPKAP kinase 2 is essential for LPS-induced TNF-alpha biosynthesis. Nat. Cell Biol. *1*, 94–97.

Kotlyarov, A., Yannoni, Y., Fritz, S., Laass, K., Telliez, J.B., Pitman, D., Lin, L.L., and Gaestel, M. (2002). Distinct cellular functions of MK2. Mol. Cell. Biol. *22*, 4827–4835.

Lee, S., Liu, B., Lee, S., Huang, S.X., Shen, B., and Qian, S.B. (2012). Global mapping of translation initiation sites in mammalian cells at single-nucleotide resolution. Proc. Natl. Acad. Sci. USA *109*, E2424–E2432.

Liang, H., He, S., Yang, J., Jia, X., Wang, P., Chen, X., Zhang, Z., Zou, X., McNutt, M.A., Shen, W.H., and Yin, Y. (2014). PTENα, a PTEN isoform translated through alternative initiation, regulates mitochondrial function and energy metabolism. Cell Metab. *19*, 836–848.

Lin, S., Choe, J., Du, P., Triboulet, R., and Gregory, R.I. (2016). The m(6)A methyltransferase METTL3 promotes translation in human cancer cells. Mol. Cell *62*, 335–345.

Malumbres, M. (2014). Cyclin-dependent kinases. Genome Biol. *15*, 122.

Menon, M.B., and Gaestel, M. (2018). MK2-TNF-signaling comes full circle. Trends Biochem. Sci. *43*, 170–179.

Menon, M.B., Ronkina, N., Schwermann, J., Kotlyarov, A., and Gaestel, M. (2009). Fluorescence-based quantitative scratch wound healing assay demonstrating the role of MAPKAPK-2/3 in fibroblast migration. Cell Motil. Cytoskeleton *66*, 1041–1047.

Menon, M.B., Schwermann, J., Singh, A.K., Franz-Wachtel, M., Pabst, O., Seidler, U., Omary, M.B., Kotlyarov, A., and Gaestel, M. (2010). p38 MAP kinase and MAPKAP kinases MK2/3 cooperatively phosphorylate epithelial keratins. J. Biol. Chem. *285*, 33242–33251.

Menon, M.B., Gropengießer, J., Fischer, J., Novikova, L., Deuretzbacher, A., Lafera, J., Schimmeck, H., Czymmeck, N., Ronkina, N., Kotlyarov, A., et al. (2017). $p38^{MAPK}$/MK2-dependent phosphorylation controls cytotoxic RIPK1 signalling in inflammation and infection. Nat. Cell Biol. *19*, 1248–1259.

Mészáros, B., Erdos, G., and Dosztányi, Z. (2018). IUPred2A: context-dependent prediction of protein disorder as a function of redox state and protein binding. Nucleic Acids Res. *46* (*W1*), W329–W337.

Modelska, A., Turro, E., Russell, R., Beaton, J., Sbarrato, T., Spriggs, K., Miller, J., Gräf, S., Provenzano, E., Blows, F., et al. (2015). The malignant phenotype in breast cancer is driven by eIF4A1-mediated changes in the translational landscape. Cell Death Dis. *6*, e1603.

Müller, S., Bley, N., Glaß, M., Busch, B., Rousseau, V., Misiak, D., Fuchs, T., Lederer, M., and Hüttelmaier, S. (2018). IGF2BP1 enhances an aggressive tumor cell phenotype by impairing miRNA-directed downregulation of oncogenic factors. Nucleic Acids Res. *46*, 6285–6303.

Oh, S., Flynn, R.A., Floor, S.N., Purzner, J., Martin, L., Do, B.T., Schubert, S., Vaka, D., Morrissy, S., Li, Y., et al. (2016). Medulloblastoma-associated DDX3 variant selectively alters the translational response to stress. Oncotarget *7*, 28169–28182.

Reinhardt, H.C., Cannell, I.G., Morandell, S., and Yaffe, M.B. (2011). Is post-transcriptional stabilization, splicing and translation of selective mRNAs a key to the DNA damage response? Cell Cycle *10*, 23–27.

Robinson, J.T., Thorvaldsdóttir, H., Winckler, W., Guttman, M., Lander, E.S., Getz, G., and Mesirov, J.P. (2011). Integrative genomics viewer. Nat. Biotechnol. *29*, 24–26.

Ronkina, N., Kotlyarov, A., Dittrich-Breiholz, O., Kracht, M., Hitti, E., Milarski, K., Askew, R., Marusic, S., Lin, L.L., Gaestel, M., and Telliez, J.B. (2007). The mitogen-activated protein kinase (MAPK)-activated protein kinases MK2 and MK3 cooperate in stimulation of tumor necrosis factor biosynthesis and stabilization of p38 MAPK. Mol. Cell. Biol. *27*, 170–181.

Ronkina, N., Menon, M.B., Schwermann, J., Arthur, J.S., Legault, H., Telliez, J.B., Kayyali, U.S., Nebreda, A.R., Kotlyarov, A., and Gaestel, M. (2011). Stress induced gene expression: a direct role for MAPKAP kinases in transcriptional activation of immediate early genes. Nucleic Acids Res. *39*, 2503–2518.

Schwermann, J., Rathinam, C., Schubert, M., Schumacher, S., Noyan, F., Koseki, H., Kotlyarov, A., Klein, C., and Gaestel, M. (2009). MAPKAP kinase MK2 maintains self-renewal capacity of haematopoietic stem cells. EMBO J. *28*, 1392–1406.

Sendoel, A., Dunn, J.G., Rodriguez, E.H., Naik, S., Gomez, N.C., Hurwitz, B., Levorse, J., Dill, B.D., Schramek, D., Molina, H., et al. (2017). Translation from unconventional 5′ start sites drives tumour initiation. Nature *541*, 494–499.

Sonenberg, N., and Hinnebusch, A.G. (2009). Regulation of translation initiation in eukaryotes: mechanisms and biological targets. Cell *136*, 731–745.

Starck, S.R., Jiang, V., Pavon-Eternod, M., Prasad, S., McCarthy, B., Pan, T., and Shastri, N. (2012). Leucine-tRNA initiates at CUG start codons for protein synthesis and presentation by MHC class I. Science *336*, 1719–1723.

Stokoe, D., Campbell, D.G., Nakielny, S., Hidaka, H., Leevers, S.J., Marshall, C., and Cohen, P. (1992). MAPKAP kinase-2; a novel protein kinase activated by mitogen-activated protein kinase. EMBO J. *11*, 3985–3994.

Thorvaldsdóttir, H., Robinson, J.T., and Mesirov, J.P. (2013). Integrative Genomics Viewer (IGV): high-performance genomics data visualization and exploration. Brief. Bioinform. *14*, 178–192.

Tiedje, C., Lubas, M., Tehrani, M., Menon, M.B., Ronkina, N., Rousseau, S., Cohen, P., Kotlyarov, A., and Gaestel, M. (2015). p38MAPK/MK2-mediated phosphorylation of RBM7 regulates the human nuclear exosome targeting complex. RNA *21*, 262–278.

Tiedje, C., Diaz-Muñoz, M.D., Trulley, P., Ahlfors, H., Laaß, K., Blackshear, P.J., Turner, M., and Gaestel, M. (2016). The RNA-binding protein TTP is a global post-transcriptional regulator of feedback control in inflammation. Nucleic Acids Res. *44*, 7418–7440.

Tyanova, S., Temu, T., Sinitcyn, P., Carlson, A., Hein, M.Y., Geiger, T., Mann, M., and Cox, J. (2016). The Perseus computational platform for comprehensive analysis of (prote)omics data. Nat. Methods *13*, 731–740.

Valentin-Vega, Y.A., Wang, Y.D., Parker, M., Patmore, D.M., Kanagaraj, A., Moore, J., Rusch, M., Finkelstein, D., Ellison, D.W., Gilbertson, R.J., et al. (2016). Cancer-associated DDX3X mutations drive stress granule assembly and impair global translation. Sci. Rep. *6*, 25996.

Waldron, J.A., Raza, F., and Le Quesne, J. (2018). eIF4A alleviates the translational repression mediated by classical secondary structures more than by G-quadruplexes. Nucleic Acids Res. *46*, 3075–3087.

Wan, J., and Qian, S.B. (2014). TISdb: a database for alternative translation initiation in mammalian cells. Nucleic Acids Res. *42*, D845–D850.

Wang, X., Zhao, B.S., Roundtree, I.A., Lu, Z., Han, D., Ma, H., Weng, X., Chen, K., Shi, H., and He, C. (2015). N(6)-methyladenosine modulates messenger RNA translation efficiency. Cell *161*, 1388–1399.

Wegrzyn, J.L., Drudge, T.M., Valafar, F., and Hook, V. (2008). Bioinformatic analyses of mammalian 5′-UTR sequence properties of mRNAs predicts alternative translation initiation sites. BMC Bioinformatics *9*, 232.

Wolfe, A.L., Singh, K., Zhong, Y., Drewe, P., Rajasekhar, V.K., Sanghvi, V.R., Mavrakis, K.J., Jiang, M., Roderick, J.E., Van der Meulen, J., et al. (2014). RNA G-quadruplexes cause eIF4A-dependent oncogene translation in cancer. Nature *513*, 65–70.

STAR★METHODS

KEY RESOURCES TABLE

REAGENT or RESOURCE	SOURCE	IDENTIFIER
Antibodies		
Rabbit monoclonal anti-MK2 (D1E11)	Cell Signaling Technology (CST)	Cat # 12155; RRID: AB_2797831
Rabbit anti-MK2	Cell Signaling Technology (CST)	Cat # 3042; RRID: AB_10694238
Rabbit monoclonal anti-phospho-MK2 (T222) (9A7)	Cell Signaling Technology (CST)	Cat # 3316; RRID: AB_2141311
Rabbit anti-phospho-MK2 (T334)	Cell Signaling Technology (CST)	Cat # 3041; RRID: AB_330726
Rabbit monoclonal anti-MK3 (D54E4)	Cell Signaling Technology (CST)	Cat # 7421; RRID: AB_10891423
Rabbit monoclonal anti-p38 (D13E1)	Cell Signaling Technology (CST)	Cat # 8690; RRID: AB_1099909
Mouse monoclonal anti-phospho-p38 (T180/Y182) (28B10)	Cell Signaling Technology (CST)	Cat # 9216; RRID: AB_331296
Rabbit monoclonal anti-phospho-Hsp27 (S82) (D1H2F6)	Cell Signaling Technology (CST)	Cat # 9709; RRID: AB_11217429
Rabbit anti-eIF4A1	Cell Signaling Technology (CST)	Cat # 2490; RRID: AB_823487
Rabbit monoclonal anti-Mettl3 (D2I6O)	Cell Signaling Technology (CST)	Cat # 96391; RRID: AB_2800261
Rabbit monoclonal anti-PTEN (138G6)	Cell Signaling Technology (CST)	Cat # 9559; RRID: AB_390810
Rabbit monoclonal anti-SRF (D71A9)	Cell Signaling Technology (CST)	Cat # 5147; RRID: AB_10694554
Rabbit anti-phospho-SRF (S103)	Cell Signaling Technology (CST)	Cat # 4261; RRID: AB_2239783
Goat anti-eEF2	Santa Cruz Biotechnology	Cat # sc-13004; RRID: AB_640040
Mouse anti-Ube2j1	Santa Cruz Biotechnology	Cat # sc-100624; RRID: AB_2210752
Mouse monoclonal anti-GFP (B-2)	Santa Cruz Biotechnology	Cat # sc-9996; RRID: AB_627695
Rabbit anti-eI2FA	Proteintech	Cat # 11233-1-AP; RRID: AB_2246321
Mouse monoclonal anti-Tubulin	Sigma-Aldrich	Cat # T6199; RRID: AB_477583
Rabbit anti-Polr1b	BiorByt	Cat # orb411900; RRID: N/A
Sheep anti-NOGO-B	R+D Systems	Cat # AF6034; RRID: AB_10573837
Mouse anti-GAPDH	EMD Millipore	Cat # MAB374; RRID: AB_2107445
Mouse monoclonal anti-RIPK1 (clone 38)	BD Biosciences	Cat # 610459; RRID: AB_397832
Mouse monoclonal anti-p150	BD Biosciences	Cat # 610473; RRID: AB_397845
Chemicals, Peptides, and Recombinant Proteins		
Anisomycin	Sigma-Aldrich	Cat # 50-76-0
MK2-Trap agarose beads	Chromotek	Cat # mta-20
p38 inhibitor Birb796 (p38i)	Axon Medchem	Cat # Axon 1358
MK2 inhibitor PF3644022 (MK2i)	Sigma-Aldrich	Cat # PZ0188
Murine recombinant Hsp25	ENZO Life Sciences	Cat # ADI-SPP-510-D
Lambda Phosphatase	New England Bioloabs (NEB)	Cat # P0753S
TRIzol Reagent	Thermo Fisher Scientific	Cat # 15596026
RiboLock RNase Inhibitor	Thermo Fisher Scientific	Cat # EO0381
RevertAid Reverse Transcriptase	Thermo Fisher Scientific	Cat # EP0441
Phos-Tag Acrylamide	FujiFilm/Wako Chemicals	Cat # AAL-107
WST-1 (water soluble tetrazolium)	Roche	Cat # 11644807001
Critical Commercial Assays		
SENSIFast SYBR Green No ROX qPCR mix	Bioline	Cat # BIO-98005
FUGene6	Promega	Cat # E2691
HiPerFect	QIAGEN	Cat # 301704
Lipofectamine RNAiMAX	Thermo Fisher Scientific	Cat # 13778150
Lipofectamine 2000	Thermo Fisher Scientific	Cat # 11668027
4-12% NuPAGE Bis-Tris Gel	Novex, Thermo Fisher Scientific	Cat # NP0321BOX

(*Continued on next page*)

Continued

REAGENT or RESOURCE	SOURCE	IDENTIFIER
Deposited Data		
RNASeq and RiboSeq of BMDMs	Tiedje et al., 2016	GEO: GSE81250
RNASeq data, HEK293	Oh et al., 2016	GEO: GSE70804
RiboSeq data, HEK293	Ingolia et al., 2012	GEO: GSE37744
RiboSeq data, BMDCs	Fields et al., 2015	GEO: GSE74139
RiboSeq data, mouse keratinocytes	Sendoel et al., 2017	GEO: GSE83332
RiboSeq data, HEK293	Valentin-Vega et al., 2016	GEO: GSE59095
RiboSeq data, Jurkat	Gawron et al., 2016	GEO: GSE74279
RiboSeq data, HCT116	Fijalkowska et al., 2017	GEO: GSE87328
MK2 nucleotide sequence data	This paper	DDBJ/ENA/GenBank TPA: BK010697
Experimental Models: Cell Lines		
Human osteosarcoma cells (U2OS)	ATCC	HTB-96; RRID:CVCL_0042
Human embryonic kidney cells (HEK293T)	ATCC	CRL-111268; RRID:CVCL_1926
Murine RAW264.7 cells	ATCC	CVCL_0493; RRID:CVCL_0493
MK2/3 double-deficient mouse embryonic fibroblasts (MEFs)	Ronkina et al., 2007	N/A
Experimental Models: Organisms/Strains		
Mouse: Mapkapk2^{tm1Mgl}	Kotlyarov et al., 1999	N/A
Mouse: Mapkapk2^{tm1Mgl}/Mapkapk3^{tm1Mgl}	Ronkina et al., 2007	N/A
Oligonucleotides		
Oligos used in this study are listed in Table S2	This paper	N/A
Recombinant DNA		
MK2 fragment for cloning (441 bp including the full murine 5′UTR)	GENEART GmbH/Thermo Fisher Scientific	N/A
pCMV-MK2-Both (WT 5′UTR)	This paper	N/A
pCMV-MK2-Short	This paper	N/A
pCMV-MK2-Long	This paper	N/A
pCMV-MK2-Super	This paper	N/A
pMMP-MK2-Both-IRES-eGFP	This paper	N/A
pMMP-MK2-Short-IRES-eGFP	This paper	N/A
pMMP-MK2-Long-IRES-eGFP	This paper	N/A
peGFP-N1-MK2-Short	This paper	N/A
peGFP-N1-MK2-Long	This paper	N/A
Software and Algorithms		
ImageJ version 1.50i	National Institute of Health (NIH), USA	https://imagej.nih.gov/ij
PRISM 8	GraphPad Software	https://www.graphpad.com/scientific-software/prism/
Galaxy Platform	Afgan et al., 2016	https://usegalaxy.org
MaxQuant software (version 1.6.0.17)	Max-Planck-Institute of Biochemistry, Munich, Germany	https://www.maxquant.org/

CONTACT FOR REAGENT AND RESOURCE SHARING

Further information and requests for resources and reagents should be directed to and will be fulfilled by the Lead Contact, Christopher Tiedje (tiedje@sund.ku.dk).

EXPERIMENTAL MODEL AND SUBJECT DETAILS

The following cell lines were primarily used in this study: Human osteosarcoma cells (U2OS), human embryonic kidney (HEK293T) cells, murine RAW264.7 cells and MK2/3 double-deficient mouse embryonic fibroblasts (MEFs), that were retrovirally rescued with different MK2 constructs. They were all cultured in DMEM medium supplemented with 10% fetal bovine serum, L-glutamine, penicillin and streptomycin at 37°C in a humidified incubator containing 5% CO_2. The cells were either obtained from ATTC or in case of the MEFs generated previously.

Handling of wild-type, MK2 knockout and MK2/3 double knockout mice (all C57BL/6J background) complied with all relevant ethical regulations and was approved by the ethics committee of the Hannover Medical School. Mice were bred and maintained at the mouse facility of the Hannover Medical School. Female mice, not older than six weeks, were used in the relevant experiments.

Information on cell lines and mouse strains can be found in the Key Resources Table.

METHOD DETAILS

Tissue culture, cell lines, treatments

Cells were grown on plates in DMEM in the presence of 10% (v/v) FCS, 100 U penicillin G/mL, and 100 mg/mL streptomycin (all purchased from Life Technologies) in a humidified atmosphere at 37°C with 5% CO_2 supplementation. Treatments with stimulators and inhibitors were done with the following final concentrations: Anisomycin, 10 μg/ml, dissolved in DMSO (Sigma); p38 inhibitor BIRB796, 1 μM, dissolved in DMSO (Axon Medchem); MK2 inhibitor PF3644022 (10 μM, Sigma) dissolved in DMSO; Cycloheximide, 20 μg/ml, dissolved in water, Sigma; Sorbitol (0,5 M, Sigma), dissolved in water; Na-Arsenite (0,5 μM, Sigma) dissolved in water; IL-1beta (2 ng/ml, Peprotech), dissolved in medium. For gene expression experiments cells were starved in serum-free medium for a minimum of 8h. MK2-deficient and MK2/3 double-deficient MEFs were described before (Ronkina et al., 2007; Ronkina et al., 2011). All other standard laboratory cell lines were either kind gifts or obtained from ATCC.

Isolation of mouse organs/bone marrow-derived macrophages

Organs of a wild-type and bone-marrow of wild-type, MK2 KO and MK2/3 DKO animals (C57BL/6J background) (Kotlyarov et al., 1999; Ronkina et al., 2007) were isolated after sacrificing them. Handling of mice complied with all relevant ethical regulations and was approved by the ethics committees of the Hannover Medical School. Organs were flash-frozen in liquid nitrogen before lysis. To derive macrophages from bone marrow after the femurs of one mouse of each genotype were flushed. Cells were then grown in the presence of 10 ng/ml M-CSF for approximately 9-10 days before using them for further experiments (Tiedje et al., 2016).

Transfection of cell lines

Cells were seeded the day before transfection to reach 50% density on the next day. The medium was then changed to penicillin/streptomycin-free. DNA was mixed in Opti-MEM (Life Technologies) and complexed with polyethylenimine (PEI, 1 μg/ml, pH 7.0, Sigma). After a minimal incubation of 10 min at room temperature the mix was added drop-wise to the cells. Medium was changed to full medium 6 h and cells were treated 24 h post-transfection and harvested.

For microscopy experiments using U2OS cells transfections were carried out according to the manufacturer using FUGene6 (Promega).

siRNA transfections

All cell lines were transfected using HiPerFect (QIAGEN), RNAiMAX (Thermo Fisher Scientific) or Lipofectamin 2000 (Thermo Fisher Scientific/Invitrogen) according to the manufacturer's instruction. The following siRNAs were used:

The sequences of all siRNAs used in this study are listed in Table S2. siRNAs were either synthesized by Eurofins/MWG or purchased from the indicated supplier.

Generation of stable shRNA knockdown cell lines

Stable HT29 cells were previously described (Menon et al., 2010). In brief, two different lentiviral particles (Mission shRNA lentiviral particles (Sigma)) and a control lentiviral particle were used. The identifiers of the shRNA particles are specified in Table S2. After transduction, cells were selected with puromycin (2 μg/mL) for 2 weeks and consequently tested for MK2 expression by Western Blot.

Cloning

A detailed description of the cloning strategy to express MK2 with its full-length 5′UTR is shown in Figure S5A. The indicated 441 bp 5′UTR-MK2 fragment having NheI and PstI sites was synthesized by GENEART GmbH (Thermo Fisher Scientific). The peGFP-C1-MK2 and pMMP-MK2-IRES-eGFP constructs for expression in mammalian cells and for retroviral transduction were described before (Ronkina et al., 2007; Schwermann et al., 2009). Point mutations were inserted by site-directed mutagenesis.

SDS-PAGE and Western Blot

If not stated differently proteins were separated on 10% SDS acrylamide gels and transferred to nitrocellulose membrane by semi-dry transfer. Phos-tag gels contained 25 μM Phos-tag stock solution (Wako Chemicals) and 0,2 μM $MnCl_2$. Before semi-dry transfer to a PVDF membrane, gels were washed three times for 30 minutes in 10 mM EDTA-containing transfer buffer. Transfer buffer contained 0,1% SDS and 1 mM EDTA. For Western Blot developments blocking and secondary antibody incubations were done for 1h at room temperature in 5% dry-milk powder dissolved in PBS containing 0.1% Tween 20 (PBS/T). Primary antibodies were usually incubated overnight at 4°C and diluted in 5% BSA dissolved in PBS/T. Antibodies to detect specific proteins: anti-MK2 (CST, #3042 and #12155), anti-pMK2^{T222} (CST, #3316), anti-pMK2^{T334} (CST, #3041), anti-MK3 (CST, #7421), anti-p38 (CST, #8690), anti-pp38$^{T180/Y182}$ (CST, #9216), anti-NOGO-B (R+D Systems, AF6034), anti-pHsp27^{S82} (CST, #9709), anti-GAPDH (EMD Millipore, #MAB374), anti-Tubulin (Sigma, #T6199), anti-eEF2 (SCBT, sc-13004), anti-p150 (BD Biosciences, #610473), anti-Mettl3 (CST, #96391), anti-eIF4A1 (CST, #2490), anti-eIF2A (Proteintech, 11233-1-AP), anti-PTEN (CST, #9559), anti-Polr1b (Biorbyt, orb411900), anti-RIPK (BD Biosciences, #610459), anti-SRF (CST, #5147), anti-pSRF^{S103} (CST, #4261), anti-Ube2j1(SCBT, sc-100624) and anti-GFP (SCBT, sc-9996). HRP-coupled secondary antibodies were used for ECL-based detection of proteins on either a LAS3000 FujiFilm or a Bio-Rad ChemiDoc Imaging System.

Protein dephosphorylation assay

Preparation of lysates was performed in the absence of phosphatase inhibitors and after clearing, the lysates were normalized by Bradford analysis. Usually 40 μl lysate was treated with 1 μl of lambda-phosphatase (NEB, 400 U/μl) for 30 minutes at 30°C in the presence of $MnCl_2$ (1 mM final) and 1 x PMP buffer (NEB) under constant agitation in an Eppendorf incubator (900 rpm). Reactions were stopped by adding 2 x SDS sample buffer.

Kinase Assay

For kinase assays MK2 isoforms were purified from one confluent 15 cm plate of the rescued MEF cell lines. For this, an agarose MK2-Trap binder (Chromotek) was used according to the manufacturer's protocol. To ensure protein purity without co-purification of other proteins, precipitates were extensively washed in MK2-Trap dilution buffer and finally resuspended in 40 μl kinase assay buffer (25 mM HEPES, pH 7.5, 25 mM $MgCl_2$, 2 mM DTT, phosphatase/protease inhibitors and 100 μM ATP). Per reaction 600 ng recombinant murine Hsp25 (1,25μg/ml, ENZO Life Sciences) were added before incubation them for 30 minutes at 30°C in an Eppendorf incubator under gentle agitation (500 rpm). Reactions were stopped by the addition of 2 x SDS sample buffer and consequent heating for 5 minutes at 95°C. Samples were then analyzed by Western Blot developing with a phospho-specific anti-Hsp27^{S82} antibody. Total, recombinant Hsp25 could be Ponceau-stained for visualization.

MK2 precipitation and LC-MS for the identification of MK2 peptides

Precipitation MK2 was done with the help of an agarose MK2-Trap binder (Chromotek) following the manufacturer's protocol. After final washing of the agarose beads, proteins were eluted using 2x SDS loading buffer and incubated for 5 min at 95°C. Eluted proteins were then alkylated by addition of acrylamide up to a concentration of 2% and incubation at room temperature for 30 min. Samples were then separated on a 10% SDS acrylamide gel. After electrophoresis proteins were stained with Coomassie Brilliant Blue (CBB) for 15 min and background staining was reduced with water. Specific MK2 lanes were excised and minced to 1 mm^3 gel pieces. Further sample processing was done as described (Jochim et al., 2011). Briefly, gel pieces were destained two times with 200 μL 50% acetonitrile (ACN), 50 mM ammonium bicarbonate (ABC) at 37°C for 30 min and then dehydrated with 100% ACN. Solvent was removed in a vacuum centrifuge and 100 μL 10 ng/μL sequencing grade Trypsin (Promega) in 10% ACN, 40 mM ABC were added. Gels were rehydrated in trypsin solution for 1 hour on ice and then covered with 10% ACN, 40 mM ABC. Digestion was performed overnight at 37°C and was stopped by adding 100 μL of 50% ACN, 0,1% trilfluoroacetic acid (TFA). After incubation at 37°C for 1 hour the solution was transferred to a fresh sample vial. This step was repeated twice and extracts were combined and dried in a vacuum centrifuge. Dried peptide extracts were redissolved in 30 μL 2% ACN, 0.1% TFA with shaking at 800 rpm for 20 min. After centrifugation at 20,000 x g aliquots of 12.5 μL each were stored at −20°C. Peptide samples were separated with a nano-flow ultra-high pressure liquid chromatography system (RSLC, Thermo Scientific) equipped with a trapping column (3 μm C18 particle, 2 cm length, 75 μm ID, Acclaim PepMap, Thermo Scientific) and a 50 cm long separation column (2 μm C18 particle, 75 μm ID, Acclaim PepMap, Thermo Scientific). Peptide mixtures were injected, enriched and desalted on the trapping column at a flow rate of 6 μL/min with 0.1% TFA for 5 min. The trapping column was switched online with the separating column and peptides were eluted with a multi-step binary gradient: linear gradient of buffer B (80% ACN, 0.1% formic acid) in buffer A (0.1% formic acid) from 4% to 25% in 30 min, 25% to 50% in 10 min, 50% to 90% in 5 min and 10 min at 90% B. The column was reconditioned to 4% B in 15 min. The flow rate was 250 nL/min and the column temperature was set to 45°C. The RSLC system was coupled online via a Nano Spray Flex Ion Soure II (Thermo Fisher Scientific) to an LTQ-Orbitrap Velos mass spectrometer. Metal-coated fused-silica emitters (SilicaTip, 10 μm i.d., New Objectives) and a voltage of 1.3 kV were used for the electrospray. Overview scans were acquired at a resolution of 60k in a mass range of m/z 300-1600 in the orbitrap analyzer and stored in profile mode. The top 10 most intensive ions of charges two or three and a minimum intensity of 2000 counts were selected for CID fragmentation with a normalized collision energy of 38.0, an activation time of 10 ms and an activation Q of 0.250 in the LTQ. Fragment ion mass spectra were recorded in the LTQ at normal scan rate and stored as centroid m/z value and intensity pairs. Active exclusion was activated so that ions fragmented

once were excluded from further fragmentation for 70 s within a mass window of 10 ppm of the specific m/z value. Raw data were processed using Proteome discoverer (Thermo Fisher Scientific) and murine uniprot/swissprot data bases containing common contaminants. Proteins were stated identified by a false discovery rate of 0.01 on protein and peptide level and quantified by extracted ion chromatograms of all peptides.

MK2 interaction profiling by label-free mass-spectrometry

Per sample 3 to 4 confluent 15 cm dishes of the corresponding MK2 MEFs were either mock-treated (DMSO), pre-treated with the MK2 inhibitor PF3644022 (10μM, Sigma) for 60 minutes or stimulated with Anisomycin (1μg/ml, Sigma) for 30 minutes before lysis. Approximately 5 mg of lysate was administered to MK2-immunoprecpitations using an agarose MK2-Trap binding resin (Chromotek). Beads were eluted in 2x Laemmli buffer and the resulting supernatants were loaded onto a 4%–12% NuPAGE Bis-Tris Gel (Novex, Thermo Fisher Scientific). Gels were then fixed and stained using the colloidal blue staining kit (Life Technologies/Invitrogen). Gel lanes were sliced into five pieces and proteins were digested in-gel using standard methods (Jensen et al., 1999). Peptides were reconstituted in 5% CAN 0.1% TFA and analyzed with an Easy-nLC 1200 system (Thermo Scientific) connected to a Fusion Lumos Orbitrap mass spectrometer (Thermo Scientific) through a nanoelectrospray ion source. Peptides were separated on a 15 cm (75 μm inner diameter) in-house column packed with 1.9 μm reversed-phase C18 beads (Reprosil-Pur AQ, Dr. Maisch), with 45 min gradients. Spray voltage was set to 2kV, capillary temperature to 275°C and RF level to 30%. A full scan was performed at a resolution of 60,000, with a scan range of 350-1400 m/z, a maximum injection time of 20 ms and with an AGC target of 500,000. Precursors were isolated with a width of 1.3 m/z and precursor fragmentation was accomplished using higher collision dissociation (HCD). Only precursors with charge state 2-5 were considered. MS/MS spectra were acquired in the Orbitrap, and settings included a loop count of 7, a maximum injection time of 118 ms and a resolution of 60,000. Raw MS data were analyzed using MaxQuant software (version 1.6.0.17). Proteins were identified with parameters previously described (Bekker-Jensen et al., 2017) and quantified using the LFQ algorithm integrated in MaxQuant (Cox et al., 2014). Match between runs function was used. Data analysis was performed using Perseus software (Tyanova et al., 2016). Missing values were imputed in all samples using Perseus default settings. Volcano plots were generated by plotting the –log10 transformed FDR-adjusted p values derived from a two-sided t test versus log2 transformed fold changed. Significance was determined based on a hyperbolic curve threshold of s0 = 0.1 using Perseus.

Migration Assay

Fibroblast migration was analyzed by a fluorescence-based scratch wound-healing assay as described previously (Menon et al., 2009).

WST-1 Assay

Cell viability assays using WST-1 (water soluble tetrazolium, Roche # 11 644 807 001) were performed as described before (Tiedje et al., 2016).

RNA extraction and qPCR

Total RNA from stimulated cells was extracted using Trizol (Thermo Fisher Scientific/Invitrogen) according to the instructions. 500 ng RNA were then reverse transcribed to cDNA using random hexameric primers and Reverse Transcriptase (Thermo Fisher Scientific) in the presence of RNase inhibitors. Quantitative PCRs (qPCRs) were performed on One Step-Plus real-time PCR systems (Applied Biosystems/Thermo Fisher Scientific) using a 2x SYBR Green no ROX qPCR mix (Bioline) in a two-step cycling program. The sequences of qPCR primer are listed in Table S2.

Microscopy

Cells were seeded on coverslips and transfected the next day using FuGENE6 (Promega) according to standard settings. The following day, cells were treated and immediately fixed with 4% PFA for 15 minutes at room temperature after washing twice with 1x PBS. Afterward, cells on coverslips were washed three times with 1x PBS before dipping them in MilliQ water and drying them. After complete drying coverslips were mounted on a glass slide in 2.5μl DAPI-containing Vector Shield (Vector Laboratories) mounting medium and fixed on the slide to avoid dissolution. Glass slides were then kept at −20°C until use. Pictures were taken on a Leica DM4 B device using the LasX Software (Leica Microsystems).

Bioinformatic analyses

The indicated datasets were analyzed using the Galaxy Suite (usegalaxy.org) (Afgan et al., 2016). In brief, raw reads were downloaded from the GEO repository, demultiplexed and converted to the FASTQ format and groomed using "FASTQ Groomer". After adapter- and quality-trimming using "Trim Galore!," the reads were mapped against human hg19 or murine mm10 using "Bowtie2". Aligned reads were then visualized in the Integrative Genomics Viewer (IGV) (Robinson et al., 2011; Thorvaldsdóttir et al., 2013).

QUANTIFICATION AND STATISTICAL ANALYSIS

Statistical analyses were performed with GraphPad PRISM 8 and in case of mass-spectrometry results with MaxQuant (version 1.6.0.17). Quantification of band intensities were carried out with the open source software ImageJ (version 1.50i). The number of biological replicates that were analyzed and the statistical tests are given in the corresponding figure legends. If not indicated differently, values are presented as mean ± SD (standard deviation). Significant differences (p values) are marked with: * ≤ 0,05, ** ≤ 0,01, *** ≤ 0,001, **** ≤ 0,0001.

DATA AND SOFTWARE AVAILABILITY

Nucleotide sequence data reported are available in the Third Party Annotation Section of the DDBJ/ENA/GenBank databases under the accession number TPA: BK010697.